Two-dimensional electronic and vibrational band structure of uniaxially strained graphene from *ab initio* calculations

Marcel Mohr,[1,*] Konstantinos Papagelis,[2] Janina Maultzsch,[1] and Christian Thomsen[1]
[1]*Institut für Festkörperphysik, Technische Universität Berlin, Hardenbergstr. 36, 10623 Berlin, Germany*
[2]*Materials Science Department, University of Patras 26504 Rio Patras, Greece*
(Received 5 October 2009; published 10 November 2009)

We present an in-depth analysis of the electronic and vibrational band structure of uniaxially strained graphene by *ab initio* calculations. Depending on the direction and amount of strain, the Fermi crossing moves away from the *K* point. However, graphene remains semimetallic under small strains. The deformation of the Dirac cone near the *K* point gives rise to a broadening of the 2D Raman mode. In spite of specific changes in the electronic and vibrational band structure the strain-induced frequency shifts of the Raman active E_{2g} and 2D modes are independent of the direction of strain. Thus, the amount of strain can be directly determined from a single Raman measurement.

DOI: 10.1103/PhysRevB.80.205410 PACS number(s): 71.15.−m, 31.15.E−, 63.22.−m

I. INTRODUCTION

The discovery of graphene in 2004 has led to strong research activities in the last years.[1] Graphene has been shown to possess unique material properties. In graphene the quantum Hall effect could be observed at room temperature.[2,3] Due to the specific band structure at the Fermi level, the electrons can be described as massless Dirac fermions.[2] Thus they mimic relativistic particles with zero rest mass and with an effective "speed of light" $c' \approx 10 \times 10^6$ m/s.[4] Due to expected ballistic transport graphene is considered to serve as building block for microelectronics. For this the graphene sheets have to be grown on an insulating material such as SiO_2 with a different lattice constant. This introduces strain, and the effect on the electronic properties is therefore extremely important. Recently, uniaxially strained graphene has been investigated by Raman spectroscopy.[5–7] The amount of strain influences the frequency of the lattice vibrations. In addition, the polarization of the Raman signal gives information on the orientation of the graphene sample.[6,7]

Theoretically the effect of uniaxial strain on the electronic properties has been investigated and the opening of a band gap has been suggested.[5,8] The question as to whether a gap opens for small strains has remained under considerable controversy.[5,9,10] The effect of hydrostatic and shear strain on the vibrational properties has been discussed in Ref. 11. Effects of uniaxial strain on the vibrational properties have been investigated *via ab initio* calculations only for very large strains on the order of 40% and only for armchair and zigzag directions.[12] In contrast, the maximum strain realized experimentally has been a few percent.[5,9,10]

Here we investigate the effect of small strains along arbitrary directions on the electronic and vibrational properties of graphene. We demonstrate that graphene remains semimetallic under strain and show how the Fermi crossing moves away from the high-symmetry points. In addition the Dirac cones become compressed. This influences the double-resonant 2D Raman mode[13,14] as the double-resonance (DR) condition is altered. The induced anisotropy leads to different DR conditions for different *k* vectors and to a broadening of the 2D peak. This broadening is on the order of 10 cm^{-1} for 1% strain when using laser lines in the visible spectrum. Although specific changes in the electronic and phononic band structure for different strain directions are found, the frequencies of the Raman active E_{2g} and 2D modes are independent of the direction of strain. Thus the amount of strain can be directly determined from a single Raman measurement.

II. METHOD

Calculations were performed with the code QUANTUM-ESPRESSO.[15] We used a plane-wave basis set, RRKJ pseudopotentials[16] and the generalized gradient approximation in the Perdew, Burke, and Ernzerhof parametrization for the exchange-correlation functional.[17] A Methfessel-Paxton broadening with a width of 0.02 Ry was used.[18] We carefully checked the convergence in the energy differences between different configurations and the phonon frequencies with respect to the wave function cutoff, the charge density cutoff, the *k*-point sampling of the Brillouin zone, the number of *q* points for calculating the dynamical matrix and the interlayer vacuum spacing for graphene. Energy differences are converged within 5 meV/atom or better, and phonon frequencies from the whole Brillouin zone within 5 cm^{-1}. The valence electrons were expanded in a plane-wave basis with an energy cutoff of 60 Ry. A $42 \times 42 \times 1$ sampling grid was used for the integration over the Brillouin zone. The dynamical matrices were calculated on a $12 \times 12 \times 1$ *q* grid using the implemented linear-response theory. Force constants were obtained via a Fourier transformation and interpolated to obtain phonons at arbitrary points in the Brillouin zone. All frequencies were multiplied by a constant factor to match the experimental Raman frequency of graphene.

III. RESULTS AND DISCUSSION

The general three-dimensional Hooke's law connects the stress tensor $\boldsymbol{\sigma}$ and the strain tensor $\boldsymbol{\epsilon}$ via the stiffness tensor $\boldsymbol{c}$: $\sigma_{ij} = c_{ijkl} \cdot \epsilon_{kl}$. As we are only interested in planar strain, the tensile strain along the *x* axis can be expressed via the two-dimensional strain tensor $\boldsymbol{\epsilon} = [(\epsilon, 0), (0, -\epsilon\nu)]$, where ν is Poisson's ratio. Since we want to apply arbitrary strain direc-

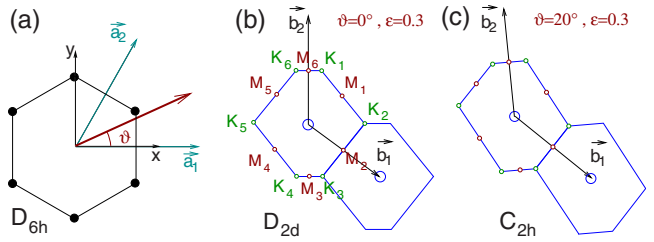

FIG. 1. (Color online) (a) The unit cell vectors $\vec{a}_1, \vec{a}_2$ of hexagonal graphene. The arrow indicates the direction of the applied strain. $\vartheta=0°$ always corresponds to the zigzag direction. (b) Brillouin zone of uniaxially strained graphene in the direction $\vartheta=0°$. The point group reduces to D_{2d}. $\vec{b}_1$ and $\vec{b}_2$ are the reciprocal lattice vectors. (c) Brillouin zone of uniaxially strained graphene in the direction $\vartheta=20°$. The point group reduces to C_{2h}.

tions the strain tensor has to be rotated $\boldsymbol{\epsilon}' = \boldsymbol{R}^{-1}\boldsymbol{\epsilon}\boldsymbol{R}$, where $\boldsymbol{R}$ is the rotational matrix. Here the x axis corresponds to the zigzag direction of graphene. After applying a finite amount of strain we relax the coordinates of the basis atoms until forces are below 0.001 Ry/a.u. and minimize the total energy with respect to the Poisson's ratio ν. For small strain values we obtain a Poisson's ratio $\nu=0.164$, in excellent agreement with experimental tension measurements on pyrolytic graphite that yield a value of $\nu=0.163$.[19] Strain reduces the symmetry of the hexagonal system. For strain in arbitrary directions the point group is reduced from D_{6h} to C_{2h}, only the C_2 rotation (rotation by 180°) and the inversion are retained (and the trivial mirror plane). For strain along the 0° or 30° directions additionally mirror planes remain, resulting in D_{2d} symmetry. A sketch of the hexagonal lattice and the corresponding strain in real space can be seen in Fig. 1(a). Due to the hexagonal symmetry only strain in the range between $\vartheta=0°$ and 30° are physically interesting.

In Figs. 1(b) and 1(c) the resulting Brillouin zones for strain in the directions 0° and 20° are shown. For clarity we have used an exaggerated strain of $\epsilon=0.3$. Like in unstrained graphene, the six corner points of the Brillouin zone correspond to the K points. In the unstrained lattice these K points, e.g., K_1 can be expressed via $K_1 = 1/3\boldsymbol{b_1} + 2/3\boldsymbol{b_2}$, where b_i are the reciprocal lattice vectors. The same definition does not hold anymore for the strained lattice, where the K points can be obtained by constructing the perpendicular bisectors to all neighboring lattice points and determine their intersection point.

The usual way to plot band structures is along the high-symmetry directions. For unstrained graphene this corresponds to Γ-K-M-Γ. In strained graphene, as the sixfold symmetry is broken these lines are not sufficient to cover all high-symmetry lines. For strain in the $\vartheta=0°$ direction we choose the lines Γ-K_2-M_2-Γ and Γ-K_3-M_3-Γ, the remaining ones can be found by symmetry. In Fig. 2 we plot the electronic band structure and the phonon dispersion curves for 2% strain and the unstrained graphene. The most obvious changes in the electronic band structure include an increase in energy of the π-type valence bands along the K-M direction. The splitting of the σ-type valence bands at $E=-3$ eV can clearly be seen. A closeup of the vicinity of the K point reveals that the crossing of the Fermi level only takes

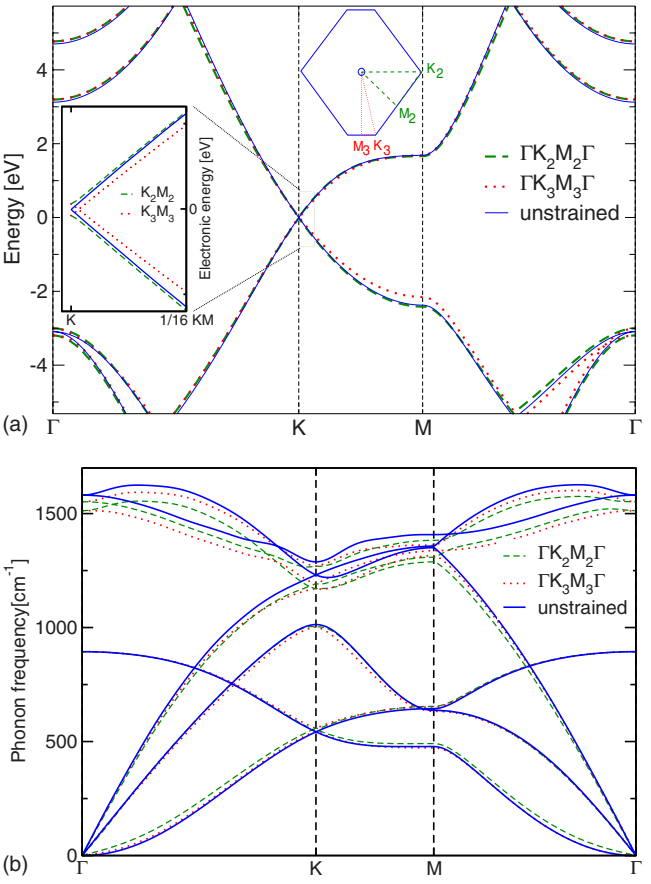

FIG. 2. (Color online) (a) The electronic band structure and (b) the phonon dispersion curves of unstrained and $\epsilon=0.02$ strained graphene along the $\vartheta=0°$-direction. The corresponding paths in the Brillouin zone are indicated. A closeup for the electronic bands along KM is shown in the inset of (a).

place between K_3 and M_3. To further investigate the position of the Fermi crossing we evaluate the direct optical transition (DOT) energy of the π-π^* bands in the vicinity of the K_1 point. In Fig. 3 we show energy contour plots of the DOT energy of the π-π^* bands. Each plot is centered at its respective K_1 point. The dimension of the sides of the square is $0.02\pi/a_0$, where a_0 is the lattice constant. We show a unstrained and a 2%-strained configuration for $\vartheta=0°$ and 20°. Although our plots show only the vicinity of the K_1 point, the remaining plots can easily be constructed. Three of the six K points are equivalent: This can be seen by apparent simple arguments: an arbitrary K point, K_i corresponds to a set of different of K points in the adjacent Brillouin zones (K_{i+2}, K_{i+4}). The equivalence to the remaining three K points follows by the C_2 rotation (or inversion), where K_i maps to K_{i+3}. Thus the contour plots of K_i $i=1,3,5$ are identical, the remaining contour plots K_i $i=2,4,6$ are found by inversion.

As can be seen, for the unstrained configuration the Dirac cones coincide with the K point. For the strained configuration at $\vartheta=0°$ the crossing moves along the K_3-M_3 line. Now the origin of the bands in Fig. 2(a) becomes clear: the line along K_2-M_2 cuts the Dirac cones away from the center, resulting in a small opening of the bands.

For the strained configuration at $\vartheta=20°$ shown in Fig. 3(c) the Fermi crossing moves away from the zone edge into

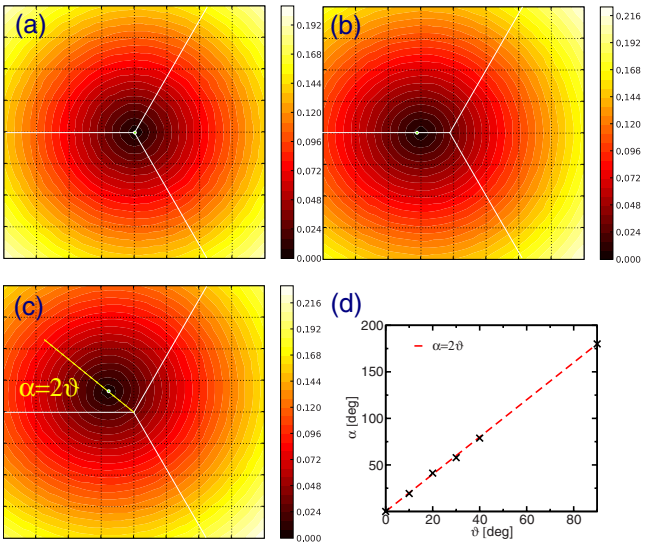

FIG. 3. (Color online) (a)–(c) Contour plots of the direct optical transition energy of the π-π^* bands. The energy is given in eV. Each is plot centered at its respective K point. The length of each side is $0.02\pi/a$. Shown here is the plot around K_1. Plots around K_i (i=3,5) are identical. K_i (i=2,4,6) can be found by inversion. (a) Unstrained configuration, (b) 2% strained configuration for ϑ=0° and (c) a 2% strained configuration for ϑ=20°. (d) Numerically obtained angle α as a function of the direction of strain ϑ. Line shows the function α=2ϑ.

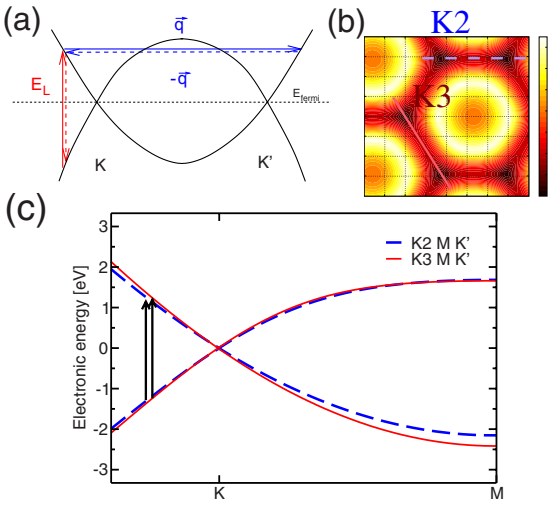

FIG. 4. (Color online) (a) Double resonance mechanism for the 2D mode. The energy of the scattering phonons is neglected. (b) Contour plot of the lowest-energy conduction band. (c) Band structure between K and K' between different K points. The corresponding paths are shown in (b). Depending on the electronic transition a different wave vector of the scattered phonon becomes resonantly enhanced. This leads to a broadening of 2D mode, as contributions from the vicinity of all K points are added up.

the Brillouin zone. The question of whether or not a gap opens in graphene under small strains must be answered by looking into the appropriate direction in reciprocal space. The tip of the Dirac cones, according to our DFT calculations, lie on lines through K that enclose an angle of α=2ϑ and the K-M line [see Fig. 3(c)]. Looking at the band structure along the strained high-symmetry directions, in contrast, corresponds to cuts of the Dirac cones not centered at the Fermi level crossing, seemingly suggesting an energy gap. This becomes important for strain in directions other than ϑ=0° and ϑ=30°, when the Fermi level does not coincide with the Brillouin zone edges.

We now turn our attention to the changes in the vibrational spectrum when strain is applied. The vibrational bands show the general trend of softening under strain. In contrast, the lowest-energy acoustic mode hardens. This mode, which shows a quadratic dependence for $q \to 0$ for unstrained graphene, is an out-of-plane mode and therefore referred to as ZA mode.[20] The hardening only occurs for the line in the Γ-K_2 direction. Also the quadratic dependence for $q \to 0$ changes into a linear dependence. This line describes propagating waves along the direction of the applied strain. Thus the hardening can be compared to the frequency increase when tension is applied to a string.

At the Γ point the high-energy E_{2g} phonon at 1581 cm^{-1} is two-fold degenerate for graphene. This degeneracy is lifted under strain. As shown in Refs. 6 and 7 the E_{2g} mode of graphene splits into two distinct modes. These two modes possess eigenvectors parallel and perpendicular to the strain direction. The mode parallel (perpendicular) to the strain direction undergoes a larger (smaller) redshift and is therefore entitled G^- (G^+). As discussed in Ref. 6 the strain rate of the G^- (G^+) mode is independent of the direction of strain, a result which we find confirmed in our calculations. This result stems from the isotropy of the hexagonal lattice.

In graphene the shape of the double-resonant 2D mode gives information on the number of layers.[21] This mode is energy dependent and double resonant.[13,14] The mechanism of a DR process is shown in Fig. 4(a). Here the phonon energy is assumed to be zero. The contributing phonon branch, the TO mode, is the mode with the highest energy between K and M [see Fig. 2(b)]. Although the 2D mode contains contributions from all over the Brillouin zone, the main contributions come from the K-K' valleys as shown by Narula and Reich.[22] Thus the one-dimensional treatment of the DR gives a good approximation.

The changes in the electronic bands and the vibrational bands both influence the 2D mode. Contour plots of the TO mode energy are shown in Fig. 5 for the unstrained and the 2% strained configuration for ϑ=0° and 20°. Each plot is centered at its respective K_1 point. Although the general shape of the vibrational mode differs more strongly than the electronic bands under strain, the stronger contribution for the shift of the 2D mode comes from changes in the electronic structure.

Figure 4(b) shows a contour plot of the lowest-energy conduction band and two different K-K' paths for the ϑ=0° direction. In Fig. 4(c) we plot the electronic bands along these two paths. Depending on the wave vector of the electronic transition a different phonon wave vector is doubly-resonant enhanced. This leads to differences in phonon energy of up to 10 $cm^{-1}/\%$ strain and explains the broadening of the 2D mode under strain.[6,7] Experimentally the broadening is found to be around 13 $cm^{-1}/\%$ strain.[6]

In Table I we show a summary of the determined shift rates for the G^+, G^-, and 2D modes. These rates are for small

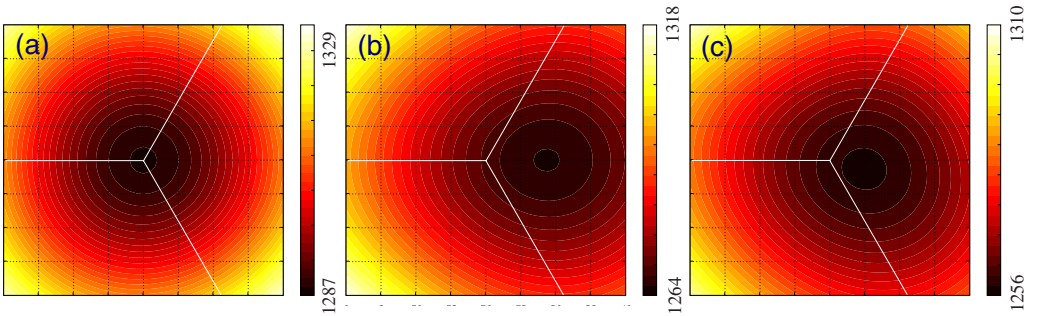

FIG. 5. (Color online) Contour plot of the fully symmetric TO phonon branch centered at the K_1 point. The TO mode contributes exclusively to the D mode. The dimension of the sides of the square is $0.2\pi/a_0$ (a) Unstrained configuration, (b) 2% strained configuration for $\vartheta=0°$ and (c) 2% strained configuration for $\vartheta=20°$.

strain values up to 2%. Our calculated values are in excellent agreement with the experimental results from Ref. 6, although the calculated values are a bit higher. In contrast to the G^+ and G^- modes, the 2D mode behaves slightly nonlinear for strain greater than 1%. Therefore we suggest to measure the G^+ and G^- modes for determining the strain rather than the 2D mode.

TABLE I. Shift rates for the G^+, the G^- and the 2D mode in strained graphene (in $\mathrm{cm}^{-1}/\%$ strain). For the excitation energy dependent 2D mode the excitation energy is written in parentheses.

Raman mode	Ref. 5	Ref. 6	Ref. 6[a]	Ref. 7	This work
G^+	−14.2	−10.8	−18.6	−5.6	−14.5
G^-	[b]	−31.7	−36.8	−12.5	−34.0
2D (2.41 eV)		−64			−46…54
2D (2.33 eV)	−27.8			−21	−46…54
2D (1.96 eV)					−46…55

[a]Rate for freestanding graphene.
[b]No distinction between G^+ and G^-.

IV. SUMMARY

In summary, we have presented an in-depth analysis of the electronic and vibrational properties of uniaxially strained graphene. We demonstrated that graphene remains semimetallic under small strain. The change in the Fermi surface suggests favored directions for electronic transport depending on the direction of strain. Our calculated shift rates of the Raman active G and 2D band will help experimentalists to determine the strain. Due to a deformation of the threefold Dirac cone around the K point the double-resonance condition changes and gives rise to a broadening of the 2D mode.

ACKNOWLEDGMENT

J.M. and C.T. acknowledge support by the Cluster of Excellence "Unifying Concepts in Catalysis" coordinated by the TU Berlin and funded by DFG.

*marcel@physik.tu-berlin.de

[1] K. S. Novoselov, A. K. Geim, S. V. Morozov, D. Jiang, Y. Zhang, S. V. Dubonos, I. V. Grigorieva, and A. A. Firsov, Science **306**, 666 (2004).
[2] K. S. Novoselov, A. K. Geim, S. V. Morozov, D. Jiang, M. I. Katsnelson, I. V. Grigorieva, S. V. Dubonos, and A. A. Firsov, Nature (London) **438**, 197 (2005).
[3] Y. Zhang, Y.-W. Tan, H. L. Stormer, and P. Kim, Nature (London) **438**, 201 (2005).
[4] K. S. Novoselov, Z. Jiang, Y. Zhang, S. V. Morozov, H. L. Stormer, U. Zeitler, J. C. Maan, G. S. Boebinger, P. Kim, and A. K. Geim, Science **315**, 1379 (2007).
[5] Z. H. Ni, T. Yu, Y. H. Lu, Y. Y. Wang, Y. P. Feng, and Z. X. Shen, ACS Nano **2**, 2301 (2008).
[6] T. M. G. Mohiuddin *et al.*, Phys. Rev. B **79**, 205433 (2009).
[7] M. Huang, H. Yan, C. Chen, D. Song, T. F. Heinz, and J. Hone, Proc. Natl. Acad. Sci. U.S.A. **106**, 7304 (2009).
[8] G. Gui, J. Li, and J. Zhong, Phys. Rev. B **78**, 075435 (2008).
[9] Z. H. Ni, T. Yu, Y. H. Lu, Y. Y. Wang, Y. P. Feng, and Z. X. Shen, ACS Nano **3**, 483 (2009).
[10] V. M. Pereira, A. H. Castro Neto, and N. M. R. Peres, Phys. Rev. B **80**, 045401 (2009).
[11] C. Thomsen, S. Reich, and P. Ordejón, Phys. Rev. B **65**, 073403 (2002).
[12] F. Liu, P. Ming, and J. Li, Phys. Rev. B **76**, 064120 (2007).
[13] C. Thomsen and S. Reich, Phys. Rev. Lett. **85**, 5214 (2000).
[14] J. Maultzsch, S. Reich, and C. Thomsen, Phys. Rev. B **70**, 155403 (2004).
[15] P. Giannozzi *et al.*, http://www.quantum-espresso.org.
[16] A. M. Rappe, K. M. Rabe, E. Kaxiras, and J. D. Joannopoulos, Phys. Rev. B **41**, 1227 (1990).
[17] J. P. Perdew, K. Burke, and M. Ernzerhof, Phys. Rev. Lett. **77**, 3865 (1996).
[18] M. Methfessel and A. T. Paxton, Phys. Rev. B **40**, 3616 (1989).
[19] O. L. Blakslee, D. G. Proctor, E. J. Seldin, G. B. Spence, and T. Weng, J. Appl. Phys. **41**, 3373 (1970).
[20] M. Mohr, J. Maultzsch, E. Dobardžić, S. Reich, I. Milošević, M. Damnjanović, A. Bosak, M. Krisch, and C. Thomsen, Phys. Rev. B **76**, 035439 (2007).
[21] A. C. Ferrari *et al.*, Phys. Rev. Lett. **97**, 187401 (2006).
[22] R. Narula and S. Reich, Phys. Rev. B **78**, 165422 (2008).